ISSN 1063-7745, Crystallography Reports, 2019, Vol. 64, No. 3, pp. 488–495. © Pleiades Publishing, Inc., 2019.
Russian Text © The Author(s), 2019, published in Kristallografiya, 2019, Vol. 64, No. 3, pp. 457–464.

CRYSTAL GROWTH

# Growth of $Sm_{1-y}Sr_yF_{3-y}$ ($0 < y \le 0.31$) Crystals and Investigation of Their Properties

**N. I. Sorokin[a], D. N. Karimov[a,*], N. V. Samsonova[a], A. G. Ivanova[a], V. A. Fedorov[a], and B. P. Sobolev[a]**

[a] *Shubnikov Institute of Crystallography, Federal Scientific Research Centre "Crystallography and Photonics," Russian Academy of Sciences, Moscow, 119333 Russia*

**e-mail: dnkarimov@gmail.com*

Received February 26, 2018; revised March 26, 2018; accepted April 23, 2018

**Abstract**—$Sm_{1-y}Sr_yF_{3-y}$ ($0 < y \le 0.31$) crystals have been grown from melt by directional solidification in a fluorinating atmosphere. The crystals have been studied by X-ray diffraction and optical spectroscopy, and their fluorine-ion conductivity $\sigma_{dc}$, density $\rho$, and refractive indices $n_D$ have been measured. It is established that $Sm^{3+}$ ions are not reduced to $Sm^{2+}$ during crystal growth. The reversible polymorphic $\alpha \leftrightarrow \beta$-$SmF_3$ transition does not make it possible to obtain bulk (>1–3 $mm^3$) samples of the tysonite phase (of $LaF_3$ type) at $y < 0.02$. The dependences $\rho(y)$ and $n_D(y)$ for the crystals are descending. The dependence $\sigma_{dc}(y)$ exhibits nonmonotonic behavior; the maximum $\sigma_{dc}$ value ($1.6 \times 10^{-4}$ S/cm) at 293 K is observed for the $Sm_{0.98}Sr_{0.02}F_{2.98}$ crystal. At $y = 0.31$, an eutectic composite $69SmF_3 \times 31SrF_2$ is formed, whose conductivity is $\sigma_{dc} = 6 \times 10^{-8}$ S/cm, a value smaller than $\sigma_{dc}$ for the crystal with $y = 0.02$ by a factor of ~$3 \times 10^3$. The carrier concentration $n_{mob}$ and its mobility $\mu_{mob}$ have been calculated for $Sm_{1-y}Sr_yF_{3-y}$ ($0.02 \le y \le 0.25$) within the hopping conductivity model. For the crystal with the highest conductivity ($Sm_{0.98}Sr_{0.02}F_{2.98}$), $n_{mob} = 4.0 \times 10^{20}$ $cm^{-3}$ and $\mu_{mob} = 2.5 \times 10^{-6}$ $cm^2/(V\,s)$ at $T = 293$ K.

**DOI:** 10.1134/S1063774519030246

## INTRODUCTION

Crystals based on fluorides of rare-earth elements (REEs) with a variable oxidation state (which include samarium, europium, and ytterbium) grown from melt in graphite containers are subjected to partial reduction ($Sm^{3+} \to Sm^{2+}$, $Eu^{3+} \to Eu^{2+}$, $Yb^{3+} \to Yb^{2+}$), the degree of which is difficult to control. As a result, data on high-temperature chemistry of trifluorides of REEs that are prone to form an atypical oxidation state ($R^{2+}$) are not as comprehensive as the data for trifluorides of other REEs, because the chemical composition of these crystals was always unclear.

Nonstoichiometric tysonite ($LaF_3$ type) $SmF_3$-based phases of $Sm_{1-y}M_yF_{3-y}$ are of interest as fluoride-conducting solid electrolytes (FSE), whose deviation from stoichiometry provided by heterovalent isomorphic substitutions of $Sm^{3+}$ with $M^{2+}$ ($M$ = Ca, Sr, or Ba). At a low reduction degree of $Sm^{3+}$ ions these crystals can be considered as pseudobinary ones.

Proceeding from the data on the partial reduction of a $SmF_3$ melt by graphite [1], researchers have tried to limit experiments on fluoride crystal growth with participation of this component. As a result, there is a lacuna in the data on $SmF_3$ (and, to a less extent, $EuF_3$ and $YbF_3$) concerning both its high-temperature chemistry and possibilities of forming and using materials with its participation. Researchers had to accept this limitation when studying Sm-containing fluoride crystals in some applications (especially photonics).

For the optimization of compositions of strongly nonstoichiometric FSEs with respect to ionic conductivity (the purpose of our study), the low impurity concentration in crystals is not very crucial; this circumstance stimulated us to carry out experiments on growing nonstoichiometric $SmF_3$-based crystals. The ion-conducting properties of a $Sm_{0.875}Sr_{0.125}F_{2.875}$ crystal were previously investigated in [2, 3]; its high electrolytic characteristics were demonstrated. The $Sm_{1-y}Sr_yF_{3-y}$ tysonite phase is interesting as a FSE, and its properties are comparable with those of well-known high-conductivity solid electrolytes $R_{1-y}Sr_yF_{3-y}$ ($R$ = La–Nd) [4–6].

Along with the applied problem of FSE optimization for new-generation current sources, this study is of great importance for the development of high-temperature chemistry of aliovalent REE fluorides and the fluoride materials science.

The chemical family of REEs is most numerous (17 elements) in the entire periodic system of elements. It is characterized by the significant effect of

the REE type on the size of $R^{3+}$ ions. These effects change nonmonotonically with an increase in the atomic number: the size increases from $Sc^{3+}$ to $Y^{3+}$ and then to $La^{3+}$; afterwards, it decreases to $Lu^{3+}$ (lanthanide compression effect). The change in the ionic radius is accompanied by three transformations of the structure type of $RF_3$ compounds (morphotropic transformations), which divide the REE trifluoride series into five structural subgroups. The correctness of phase diagrams with participation of $RF_3$, which underlie the fluoride materials science involving REE ions (which are of great practical importance in many fields of physics), depends on the structure type, presence (absence) of polymorphic transformations in compounds of these subgroups, and phase-transition temperatures.

The first morphotropic transition in the $RF_3$ series is in the portion of the series covering Pm, Sm, and Eu. It turned out that fluorides of all these REEs have limitations for experimental studies. Promethium fluoride is inaccessible because of natural radioactivity, while samarium and europium fluorides have hardly been fabricated for practical applications because of their partial reduction. As a result, three REEs in succession were excluded from the series, which significantly hindered the interpolation of properties of Sm, Pm, and Eu compounds, a procedure that nicely works specifically for REEs in small portions of the series.

Under the conditions conventional for thermal analysis of the heating rates in nominally pure $SmF_3$, there is a reversible phase transition from the nonconducting orthorhombic β form (sp. gr. *Pnma*, $Z = 4$) to the low-temperature fluoride-conducting tysonite form α-*l*-$SmF_3$ (sp. gr. $P\bar{3}c1$, $Z = 6$).

Note that the tysonite-type structure has two forms: trigonal (sp. gr. $P\bar{3}c1$, $Z = 6$) and hexagonal (sp. gr. $P6_3/mmc$, $Z = 2$), which were distinguished in [7]; according to these data, these forms correspond to high- and low-temperature forms, respectively. A transition between them can be assigned to the diffuse type, which affects only one (anion) sublattice. A similar transition, observed for compounds with the fluorite-type structure, is not a reconstructive polymorphic transformation. To distinguish the diffuse transition (between forms) and the polymorphic transition (between modifications), we decided to retain the generally accepted designations of modifications with Greek letters (α, β). Different types of the tysonite (in our case) structure are denoted in accordance with the their temperature stability regions: *h* (high-temperature) and *l* (low-temperature) forms. They slightly differ in X-ray powder diffraction patterns, are not always determined in studies, and may coexist in one crystal. When these forms are determined (as in this paper), one should use double designations (including modification and form).

In view of the aforesaid, the tysonite modification α-$SmF_3$ undergoes, in turn, a diffuse transition from the low-temperature form α-*l*-$SmF_3$ (sp. gr. $P\bar{3}c1$, $Z = 6$) to the high-temperature form α-*h*-$SmF_3$ (sp. gr. $P6_3/mmc$, $Z = 2$) at $T \sim 1100$°C [8]. Among two REEs (Sm and Eu), the polymorphic transition in $EuF_3$ occurs at 852 ± 8°C [7] (i.e., in the temperature range where the bulk diffusion is unfrozen), and its presence is well proven by thermal analysis. In $SmF_3$ (the melting temperature is $T_m = 1304 \pm 10$°C [7] and the freezing threshold of bulk diffusion is ~540°C), the phase polymorphic transformation is near 495°C [8], where the bulk diffusion is frozen. This leads to a spread of several tens of kelvins between the transformation temperatures obtained by different researchers [9]. As a result, it is difficult to locate reliably the morphotropic transition between $PmF_3$ and $SmF_3$.

A practical goal of our investigation was to obtain a concentration series of $Sm_{1-y}Sr_yF_{3-y}$ tysonite crystals, the growth of which had been hindered for a long time by considerations about the presence of destructive polymorphic $\alpha \leftrightarrow \beta$ transformation in $SmF_3$; this problem was methodically solved for the first time.

Much interest in $R_{1-y}M_yF_{3-y}$ tysonite crystals ($M$ = Sr or Ba, $R$ is a REE) has been shown only recently, after the great progress in the design of new fluorine-ion current sources, which can compete now with lithium-ion current sources in many parameters [10–14].

The purpose of this study was to grow $Sm_{1-y}Sr_yF_{3-y}$ tysonite-phase crystals and $69SmF_3 \times 31SrF_2$ eutectic composition from melt; characterize them by X-ray diffraction (XRD) analysis and optical spectroscopy; and investigate the concentration dependences of fluorine-ion conductivity $\sigma_{dc}(y)$, density $\rho(y)$, and refractive index $n_D(y)$.

## EXPERIMENTAL

### *Crystal Growth and Preparation of a Eutectic Composite*

The phase diagram of the $SrF_2$–$SmF_3$ system [15] is shown in Fig. 1. This system belongs to the eutectic type with the following eutectics coordinates: temperature 1312 ± 10°C and composition 69 ± 2 mol % $SmF_3$. The growth of crystals of the $Sr_{1-x}Sm_xF_{2+x}$ fluorite phase (phase **F** in Fig. 1) and their complex characterization were presented in [16, 17]. The addition of $SrF_2$ to $SmF_3$ leads to the formation of the $Sm_{1-y}Sr_yF_{3-y}$ nonstoichiometric phase with a tysonite-type defect structure ($LaF_3$), in which the $SrF_2$ content varies in the range of 0–23 mol % at the eutectic temperature (phase **T** in Fig. 1). A temperature maximum (1340 ± 10°C) is observed in the liquidus curves of the $Sm_{1-y}Sr_yF_{3-y}$ phase for the composition with 13 mol % $SrF_2$ (mole fraction $y \approx 0.13$),

which exceeds the melting temperature of the component $SmF_3$ by ~35°C.

The growth experiments were carried out using compositions $Sm_{1-y}Sr_yF_{3-y}$ with the $SrF_2$ content in the range of $y = 0$–$0.31$. The $Sm_{1-y}Sr_yF_{3-y}$ crystals and $69SmF_3 \times 31SrF_2$ composite were grown by directional solidification in a two-zone system with resistive heating and a graphite heating unit in a mixed atmosphere of high-purity helium and $CF_4$ (up to 50 vol %). The initial agents were $SmF_3$ (purity 99.99 wt %, LANHIT) and $SrF_2$ (purity 99.995 wt %, Sigma-Aldrich) powders. Multicellular graphite crucibles with seed capillary channels were used. The temperature gradient in the growth zone was ~80°C/cm. The crucible pulling rate was ~3 mm/h. The mean crystal cooling rate after the growth was 100°C/h. The evaporation loss did not exceed 0.5–0.8 wt %.

*X-ray diffraction analysis* was performed with a Rigaku MiniFlex 600 X-ray powder diffractometer (radiation $CuK_\alpha$). X-ray diffraction patterns were recorded in the range of 2θ angles from 10° to 100°. The phases were identified using the ICDD PDF-2 (2014) database. The unit-cell parameters were refined by the Rietveld method using the X'Pert HighScore Plus software (PANanalytical, the Netherlands).

Samples with a thickness of $h = 2$ mm for the investigations were cut from the central portions of the $Sm_{1-y}Sr_yF_{3-y}$ crystals ($0.03 \le y \le 0.31$) and polished. The sample with $y = 0.02$ was $1 \times 3 \times 3$ mm$^3$ in size.

*Crystal density* ρ was measured by hydrostatic weighing in distilled water at room temperature with an error of $\Delta\rho = \pm 0.005$ g/cm$^3$.

*Refractive indices* $n_D$ (wavelength $\lambda = 0.589$ μm) were investigated by the refractometric method (immersion liquid α-bromonaphthalene) at room temperature using an IRF-454 refractometer.

*Optical transmission spectra* of the crystals were recorded at room temperature with a Cary 5000 spectrophotometer (Agilent Technologies) and a Nicolet Nexus 5700 IR Fourier spectrometer (Thermo Scientific) in the wavelength range of $\lambda = 0.2$–$15$ μm.

*Electrical measurements* were performed on unoriented samples because the anisotropy of conductivity of crystals of the tysonite nonstoichiometric phases can be neglected [18, 19]. Inert electrodes were made of graphite paste Dag-580 (Acheson Colloids). Dc electrical conductivity $\sigma_{dc}$ was determined by impedance spectroscopy. The technique of electrical measurements was reported in [20]. The relative error in measuring $\sigma_{dc}$ was 5%.

Complex impedance $Z^*(\omega)$ of the concentration series of $Sm_{1-y}Sr_yF_{3-y}$ crystals at room temperature ($T = 293$ K) was measured in the frequency range of $5$–$5 \times 10^5$ Hz and at resistances from 1 to $10^7$ Ω (impedancemeter Tesla BM–507) in a vacuum (~1 Pa).

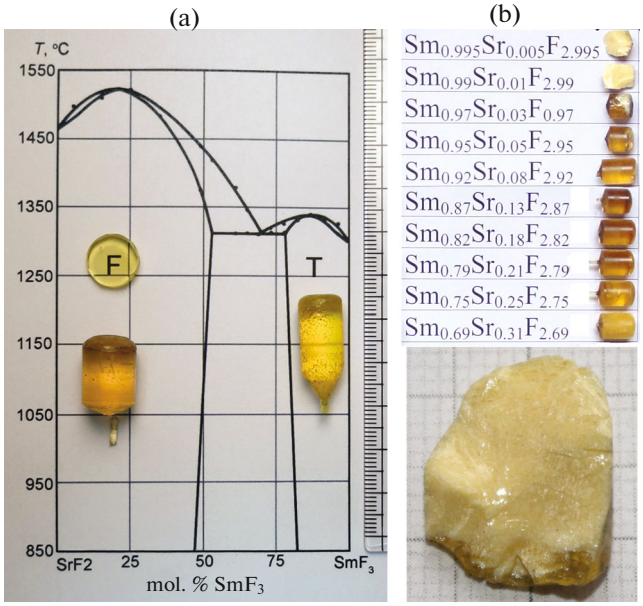


**Fig. 1.** (Color online) (a) Phase diagram of the $SrF_2$–$SmF_3$ system. The crystals obtained from the compositions of maxima for the fluorite (**F**) and tysonite (**T**) phases are presented. (b) Appearance of the series of samples $Sm_{1-y}Sr_yF_{3-y}$ and $Sm_{0.995}Sr_{0.005}F_{2.9995}$.

Temperature investigations of impedance $Z^*(\omega)$ for the $Sm_{0.97}Sr_{0.03}F_{2.97}$ crystal and $69SmF_3 \times 31SrF_2$ eutectic composite were carried out in the temperature range of 290–541 K.

The presence of the blocking effect from inert (graphite) electrodes in the low-frequency impedance spectra indicates the ionic character of electrotransfer in the crystals. For the $69SmF_3 \times 31SrF_2$ eutectic composite, the total conductivity of the sample was found; it was not separated into bulk and intercrystallite contributions.

## RESULTS AND DISCUSSION

We prepared 14 $Sm_{1-y}Sr_yF_{3-y}$ crystal boules 12 mm in diameter and 25–35 mm long with a content of $0.005 \le y \le 0.31$ (Fig. 1b). Crystals with $0.03 \le y \le 0.21$ had no cracks and bulk inclusions. For the samples with $0.005 \le y \le 0.02$, the transparent phase was observed only at the bottom of the boules and was less than 2% of the total length. A semitransparent rejected phase was observed at the top of the crystal for compositions in the range of $0.18 \le y \le 0.25$; the sample with $y = 0.31$ had two phases and was visually semitransparent. Note that the $Sm_{1-y}Sr_yF_{3-y}$ samples with $0.005 \le y \le 0.02$ were stuck in the graphite crucible cells. This mechanical sticking of $Sm_{1-y}Sr_yF_{3-y}$ crystals is caused by the β-$SmF_3$ (sp. gr. *Pnma*) ↔ α-*l*-$SmF_3$ (sp. gr. $P\bar{3}c1$) polymorphic transition accompanied by a decrease in the density.

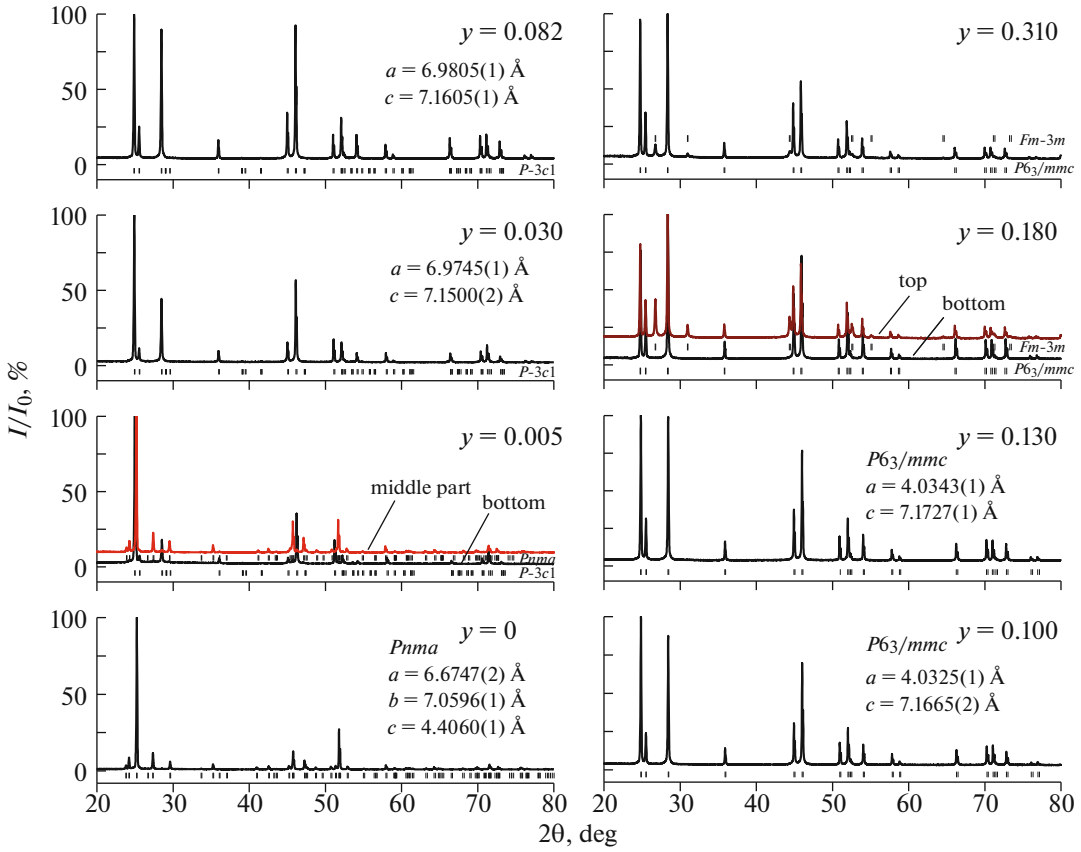


**Fig. 2.** X-ray diffraction patterns of the $Sm_{1-y}Sr_yF_{3-y}$ samples. Positions of the Bragg reflections for the phases of indicated space groups are shown.

An XRD analysis of the $Sm_{1-y}Sr_yF_{3-y}$ crystals showed that they are single-phase throughout the entire volume for the compositions of $0.03 \le y \le 0.18$ (Fig. 2). $Sm_{1-y}Sr_yF_{3-y}$ crystal boules with $0.005 \le y \le 0.02$ are two-phase. Opaque upper regions of these boules (Fig. 1a) correspond to the orthorhombic β-$SmF_3$ phase (sp. gr. *Pnma*), while the transparent regions correspond to the tysonite phase α-*l*-$Sm_{1-y}Sr_yF_{3-y}$ (sp. gr. $P\bar{3}c1$). The low-temperature phase α-*l*-$Sm_{1-y}Sr_yF_{3-y}$ is formed during the crystallization of compositions with $0.005 \le y \le 0.08$. The compositions with $y > 0.08$ exhibit a transition from the tysonite form α-*l*-$Sm_{1-y}Sr_yF_{3-y}$ (sp. gr. $P\bar{3}c1$) to the high-temperature form α-*h*-$Sm_{1-y}Sr_yF_{3-y}$ (sp. gr. $P6_3/mmc$) and its stabilization.

The semitransparent rejected substance at the top of the $Sm_{1-y}Sr_yF_{3-y}$ samples for $0.18 \le y \le 0.25$ consists of a mixture of the "impurity" fluorite phase $Sr_{1-x}Sm_xF_{2+x}$ (sp. gr. $Fm\bar{3}m$) with the unit-cell parameter $a = 5.775(1)$ Å and the primary tysonite phase α-*h*-$Sm_{1-y}Sr_yF_{3-y}$, which is in agreement with the limiting solubility of $SrF_2$ in the $SmF_3$ matrix ($y \approx 0.23$) obtained in [15].

The sample with $y = 0.31$ was a two-phase (throughout the entire volume) eutectic composite consisting of a mixture of nonstoichiometric phases with boundary compositions for the fluorite (sp. gr. $Fm\bar{3}m$, $a = 5.774(1)$ Å) and tysonite (sp. gr. $P6_3/mmc$, $a = 4.0419(1)$ Å, $c = 7.1951(1)$ Å) structures.

Figure 3 shows the concentration dependences of the lattice parameters $a(y)$ and $c(y)$ and unit-cell volume $V$ of the $Sm_{1-y}Sr_yF_{3-y}$ nonstoichiometric-phase crystals. These data are in satisfactory agreement with the results of [21]. The parameter $c(y)$ increases according to a weak quadratic law from 7.1323(1) to 7.1951(1) Å in the composition range of $0.005 \le y \le 0.31$. In the range of $y = 0.08$–$0.10$ A, one can clearly see a change in the form of the tysonite-type structure and a transition from a "large cell" (α-*l*-$Sm_{1-y}Sr_yF_{3-y}$, sp. gr. $P\bar{3}c1$, $Z = 6$) to a "small cell" (α-*h*-$Sm_{1-y}Sr_yF_{3-y}$, sp. gr. $P6_3/mmc$, $Z = 2$). The observed concentration-driven structural transition with a change in the unit-cell volume and space symmetry group is characteristic of $R_{1-y}M_yF_{3-y}$ tysonite nonstoichiometric phases ($R$ = La–Nd, $M$ = Ca, Sr, or Ba) [22, 23].

*The results of measuring density* ρ($y$) of the $Sm_{1-y}Sr_yF_{3-y}$ tysonite-phase crystals are shown in Fig. 4a. The

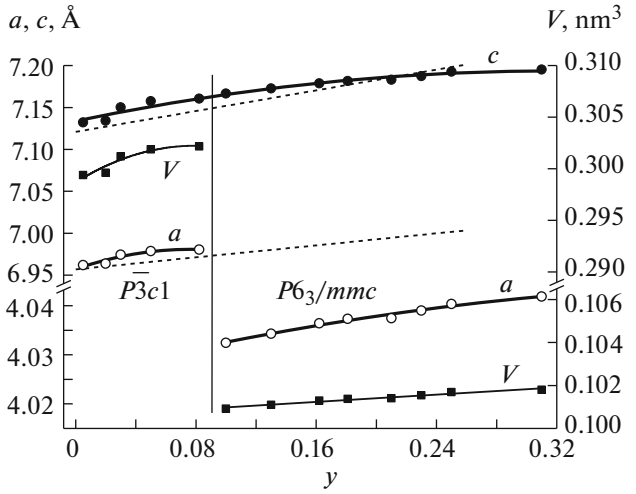


**Fig. 3.** Concentration dependences of the lattice parameters (○, ●) and unit-cell volumes (■) of the $Sm_{1-y}Sr_yF_{3-y}$ tysonite phase. The dotted lines are analytical dependences $a(y)$ and $c(y)$ according to the data of [21].

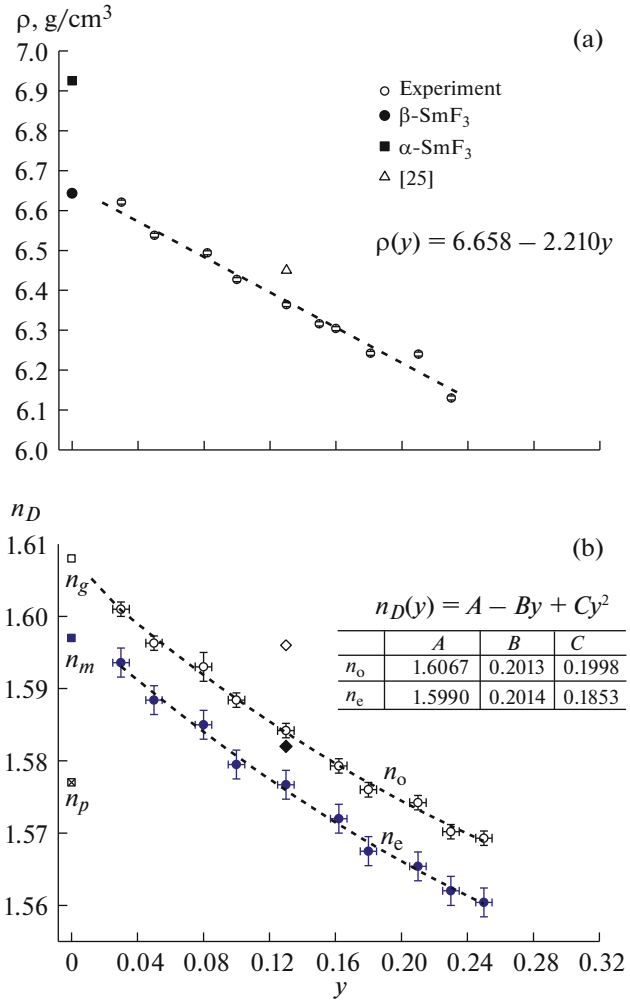


**Fig. 4.** Concentration dependences of the (a) density and (b) refractive indices for the $Sm_{1-y}Sr_yF_{3-y}$ crystals at $T = 293$ K. Designations are as follows: (a) (○) the experimental values; (■,●) the X-ray density for, respectively, α-$SmF_3$ and β-$SmF_3$ [24]; and (Δ) the data of [25] for $Sm_{0.87}Sr_{0.13}F_{2.87}$)); (b) (○, ●) the experimental values for $n_o$ and $n_e$, respectively; (◇, ◆) $n_o$ and $n_e$, respectively, for $Sm_{0.87}Sr_{0.13}F_{2.87}$ at $\lambda = 0.635$ μm [25]; and (□, ■, ⊠) the principal refractive indices for β-$SmF_3$ [26].

dependence $\rho(y)$ has a practically linear (with an error of $\Delta\rho = \pm 0.02$ g/cm$^3$) descending character in the range of $0.03 \le y \le 0.23$. The data on the densities of the tysonite α-*l*-$SmF_3$ and orthorhombic β-$SmF_3$ modifications [24] and the $Sm_{0.87}Sr_{0.13}F_{2.87}$ crystal [25] are shown for comparison.

*Dependences of the refractive indices* $n_D$ of $Sm_{1-y}Sr_yF_{3-y}$ crystals on the composition ($0.03 \le y \le 0.25$) are shown in Fig. 4b. The crystals are uniaxial and optically negative ($n_o > n_e$). The $n_o$ values at wavelength $\lambda = 0.589$ μm decrease monotonically from 1.601(1) to 1.569(1) in the composition range $y$ under consideration. The dependences $n_D(y)$ can be described by second-order polynomials, whose parameters are given in Fig. 4b. The birefringence is $\Delta n_D \sim 0.008$; it barely depends on the crystal composition $y$. As can be seen in Fig. 4b, the optical data for the Czochralski-grown $Sm_{0.87}Sr_{0.13}F_{2.87}$ crystal [25] differ significantly from our data, which likely indicates an error in determining its chemical composition. The principal refractive indices of the β-$SmF_3$ crystal [26] are given for comparison.

*Optical transmission spectra* of the $Sm_{1-y}Sr_yF_{3-y}$ crystals are shown in Fig. 5. The crystals are transparent in the IR range up to 13 μm. The spectra exhibit transitions from the ground $^6H_{5/2}$ state to the above multiplets of the $4f^5$ $Sm^{3+}$ configuration. Absorption bands caused by the $4f^5$–$4f5d^1$ transitions (which are characteristic of $Sm^{2+}$ ions) are located in the visible and UV spectral regions [27]. For comparison, Fig. 5 (curve *3*) shows a transmission spectrum of the $La_{0.99}Sm_{0.01}F_3$ crystal grown in a reducing atmosphere. The spectrum of this crystal exhibits absorption at $\lambda < 0.7$ μm, which indicates the presence of a fraction of reduced $Sm^{2+}$ ions, which was not observed for the $Sm_{1-y}Sr_yF_{3-y}$ crystals under study. Thus, under the redox conditions of growing $Sm_{1-y}Sr_yF_{3-y}$ crystals from melt in graphite crucibles that were implemented in our experiments, there is no significant reduction of $Sm^{3+}$ ions to state 2+.

*The concentration dependence of the fluorine-ion conductivity* of the $Sm_{1-y}Sr_yF_{3-y}$ tysonite-phase crystals ($0.02 \le y \le 0.25$) has decays monotonically (Fig. 6). The maximum conductivity ($\sigma_{dc} = 1.6 \times 10^{-4}$ S/cm) was found for the $Sm_{0.98}Sr_{0.02}F_{2.98}$ crystal. Its conductivity is about 3 times lower than that of the

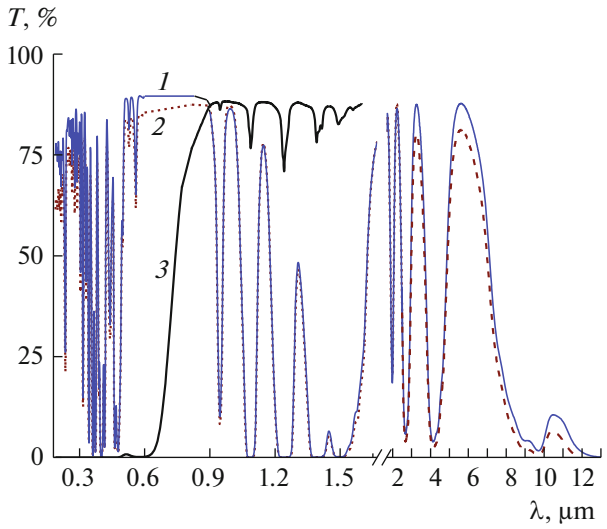


**Fig. 5.** (Color online) Transmission spectra of the $Sm_{1-y}Sr_yF_{3-y}$ crystals for $y = (1)$ 0.13 and (2) 0.18 and (3) the $La_{0.99}Sm_{0.01}F_3$ crystal grown under reducing conditions. The samples are 2 mm thick.

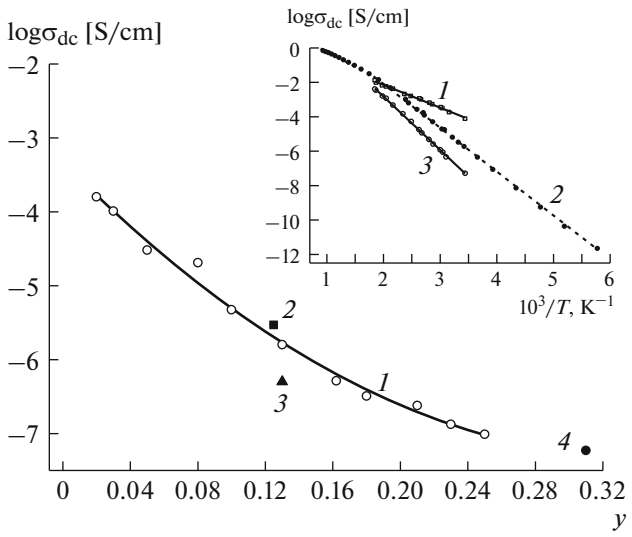


**Fig. 6.** Concentration dependences of the ionic conductivity $\sigma_{dc}(y)$ for the (1–3) $Sm_{1-y}Sr_yF_{3-y}$ crystals and (4) $69SmF_2 \times 31SrF_2$ composite at $T = 293$ K: (1, 4) this study, (2) [6], and (3) [28]. The temperature dependences of the ionic conductivity $\sigma_{dc}(T)$ for the (1) $Sm_{0.97}Sr_{0.03}F_{2.97}$ and (2) $Sm_{0.875}Sr_{0.125}F_{2.875}$ [6] crystals and (3) $69SmF_2 \times 31SrF_2$ composite are shown in the inset.

$Ce_{0.97}Sr_{0.03}F_{2.97}$ crystal, which has the highest conductivity in the $R_{1-y}Sr_yF_{3-y}$ system [3, 5]. The conductivity of the $69SmF_3 \times 31SrF_2$ eutectic composite is $\sigma_{dc} = 6 \times 10^{-8}$ S/cm, which is much smaller (by a factor of $2.7 \times 10^3$) than the $\sigma_{dc}$ value for the $Sm_{0.98}Sr_{0.02}F_{2.98}$ crystal. For comparison, Fig. 6 shows data on the conductivity of $Sm_{1-y}Sr_yF_{3-y}$ crystals ($y = 0.125$ [6] and 0.13 [28]).

The temperature dependences of the ionic conductivity $\sigma_{dc}(T)$ for the $Sm_{0.97}Sr_{0.03}F_{2.97}$ crystal and $69SmF_2 \times 31SrF_2$ eutectic composite in the temperature range of 290–541 K are shown in the inset in Fig. 6 (curves *1*, *3*). The dependence $\sigma_{dc}(T)$ were processed using the Frenkel–Arrhenius equation:

$$\sigma_{dc}(T) = A\exp(-\Delta H_\sigma/kT), \quad (1)$$

where $A$ is the pre-exponential factor of conductivity, $\Delta H_\sigma$ is the ion-transport activation enthalpy, $k$ is the Boltzmann constant, and $T$ is temperature. The Frenkel–Arrhenius equation parameters are as follows: $A = 3.5 \times 10^3$ S K/cm and $\Delta H_\sigma = 0.30 \pm 0.03$ eV for the $Sm_{0.97}Sr_{0.03}F_{2.97}$ crystal and $A = 2.7 \times 10^6$ S K/cm and $\Delta H_\sigma = 0.65 \pm 0.02$ eV for the $69\ SmF_2 \times 31SrF_2$ composite.

For comparison, the dependence $\sigma_{dc}(T)$ for the congruently melting $Sm_{0.875}Sr_{0.125}F_{2.875}$ crystal studied previously in [6] in a wide temperature range (173–1073 K) is shown in the inset in Fig. 6 (curve *2*). In this range, $\sigma_{dc}$ increases from $2 \times 10^{-12}$ to $7 \times 10^{-1}$ S/cm (i.e., by 11 orders of magnitude). At 573 K, the dependence $\sigma_{dc}(T)$ is divided into two portions. The Frenkel–Arrhenius equation parameters for them are as follows: $A = 9.1 \times 10^5$ S K/cm and $\Delta H_\sigma = 0.53 \pm 0.01$ eV at 173–573 K and $A = 5.6 \times 10^4$ S K/cm and $\Delta H_\sigma = 0.39 \pm 0.02$ eV at 573–1073 K.

The results of studying the $R_{1-y}M_yF_{3-y}$ tysonite phases in the $MF_2$–$RF_3$ systems ($M$ = Ca, Sr, or Ba) by the $^{19}F$ NMR method [29–31] indicate that ion transport therein occurs in the anion sublattice. The mechanism of ionic conductivity in $R_{1-y}M_yF_{3-y}$ crystals is related to the migration of fluorine vacancies $V_F^+$; no defect clusters were found [2–6, 28, 32–34].

Heterovalent substitutions in the $Sm_{1-y}Sr_yF_{3-y}$ cation sublattice induce mobile fluorine vacancies in the anion sublattice:

$$Sm^{3+} \rightarrow Sr^{2+} + V_F^+, \quad (2)$$

where $V_F^+$ is the ion charge carrier. The ion transport in the $Sm_{1-y}Sr_yF_{3-y}$ crystals is determined by the characteristics of mobile vacancies $V_F^+$:

$$\sigma_{dc} = qn_{mob}\mu_{mob}, \quad (3)$$

where $q$, $n_{mob}$, and $\mu_{mob}$ are, respectively, the charge, concentration, and mobility of vacancies $V_F^+$. The charge-carrier concentration in ion conductors $R_{1-y}M_yF_{3-y}$ is temperature-independent and determined by the mechanism of formation of "impurity" vacancies (2). Considering the structural data, we calculated the concentration of carriers,

$$n_{mob} = 2Zy/(\sqrt{3}a^2c), \quad (4)$$

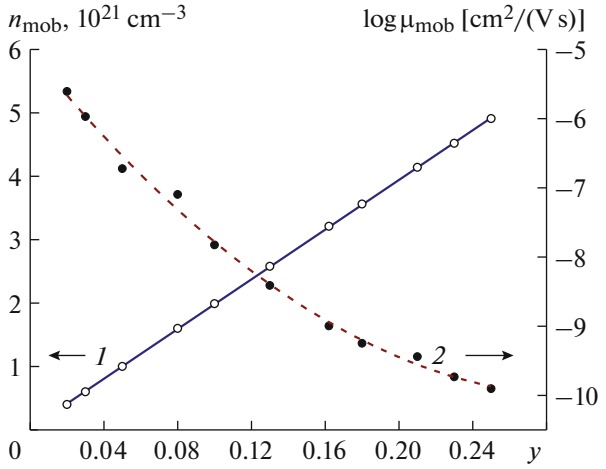


**Fig. 7.** (Color online) Dependences of the (*1*) concentration $n_{mob}(y)$ and (*2*) mobility $\mu_{mob}(y)$ at $T = 293$ K for the $Sm_{1-y}Sr_yF_{3-y}$ crystals on the $SrF_2$ content.

and then, using (3) and (4), determined their mobility $\mu_{mob}$.

The calculated $n_{mob}$ and $\mu_{mob}$ values for the $Sm_{1-y}Sr_yF_{3-y}$ crystals are presented in Fig. 7. The charge-carrier concentration at $T = 293$ K for the crystal with the highest conductivity ($Sm_{0.98}Sr_{0.02}F_{2.98}$) is $n_{mob} = 4.0 \times 10^{20}$ cm$^{-3}$ at the mobility $\mu_{mob} = 2.5 \times 10^{-6}$ cm$^2$/(V s). When the $SrF_2$ content increases, the dependences $n_{mob}(y)$ and $\mu_{mob}(y)$ behave differently. The $n_{mob}$ values increase by a factor of 12 with an increase in $y$ from 0.02 to 0.25, whereas the $\mu_{mob}$ values decrease by a factor of $2 \times 10^4$. The decrease in $\sigma_{dc}$ for the $Sm_{1-y}Sr_yF_{3-y}$ crystals in the composition range of $0.02 \le y \le 0.25$ is caused by a decrease in the carrier mobility due to ion–ion interactions between carriers.

## CONCLUSIONS

A series of $Sm_{1-y}Sr_yF_{3-y}$ crystals ($0 < y \le 0.31$) was grown from melt by the Bridgman method for the first time. It was shown that the $\alpha \leftrightarrow \beta$ polymorphic transformation in $SmF_3$ does not make it possible to prepare bulk $Sm_{1-y}Sr_yF_{3-y}$ tysonite-phase samples (type $LaF_3$) for the compositions of $y < 0.02$. Under the implemented conditions of growing $Sm_{1-y}Sr_yF_{3-y}$ crystals from melt in a graphite crucible in a fluorinating atmosphere ($CF_4$), no significant reduction of $Sm^{3+}$ ions to $Sm^{2+}$ occurred.

The low-temperature $\alpha$-*l*-$Sm_{1-y}Sr_yF_{3-y}$ tysonite phase (sp. gr. $P\bar{3}c1$) is formed for the $Sm_{1-y}Sr_yF_{3-y}$ crystals with $0.005 \le y \le 0.08$. Beginning with the content of $y > 0.08$, X-ray diffraction analysis revealed stabilization of the high-temperature $\alpha$-*h*-$Sm_{1-y}Sr_yF_{3-y}$ tysonite phase (sp. gr. $P6_3/mmc$). The sample with $y = 0.31$ is a two-phase eutectic composite consisting of a mixture of nonstoichiometric phases with saturated (at the eutectic temperature) compositions for the fluorite ($Sr_{1-x}Sm_xF_{2+x}$) and tysonite ($Sm_{1-y}Sr_yF_{3-y}$) structures.

It was established that the concentration transition in the tysonite modifications ($\alpha$-*l*-$Sm_{1-y}Sr_yF_{3-y} \leftrightarrow \alpha$-*h*-$Sm_{1-y}Sr_yF_{3-y}$) at $y = 0.08$–$0.1$ does not manifest itself in the concentration dependences of density $\rho(y)$, refractive index $n_D(y)$, and conductivity $\sigma_{dc}(y)$. For the nonstoichiometric $Sm_{1-y}Sr_yF_{3-y}$ tysonite phase ($0.03 \le y \le 0.25$), the density $\rho(y)$ and refractive index $n_D(y)$ monotonically decrease in the composition range of $0.03 \le y \le 0.25$.

The concentration dependence of the ionic conductivity was investigated for the $Sm_{1-y}Sr_yF_{3-y}$ nonstoichiometric-phase crystals in the composition range of $0.02 \le y \le 0.25$ and the $69SmF_2 \times 31SrF_2$ composite. The room-temperature conductivity of the $69SmF_2 \times 31SrF_2$ eutectic composite is $\sigma_{dc} = 6 \times 10^{-8}$ S/cm; for the most conducting solid-solution crystal, $Sm_{0.98}Sr_{0.02}F_{2.98}$ ($y = 0.02$), $\sigma_{dc} = 1.6 \times 10^{-4}$ S/cm.

Within the hopping-conductivity model, the concentration and mobility of carriers (fluorine vacancies) were calculated for the $Sm_{1-y}Sr_yF_{3-y}$ crystals; their values for the $Sm_{0.98}Sr_{0.02}F_{2.98}$ crystal are, respectively, $n_{mob} = 4.0 \times 10^{20}$ cm$^{-3}$ and $\mu_{mob} = 2.5 \times 10^{-6}$ cm$^2$/(V s) ($T = 293$ K). The antibatic behavior of dependences $n_{mob}(y)$ and $\mu_{mob}(y)$ determines the decrease in the $\sigma_{dc}$ value of the $Sm_{1-y}Sr_yF_{3-y}$ crystals with an increase in the content $y$.

## ACKNOWLEDGMENTS

We are grateful to N.A. Ivanovskaya, B.V. Nabatov, and T.B. Kosova for their help in carrying out experiments.

## FUNDING

This study was supported by the Russian Foundation for Basic Research, project nos. 16-03-00707 and 17-00-00118, in the part concerning growth of crystals and by the Ministry of Higher Education and Science of the Russian Federation within the State assignment in the part concerning the analysis of crystal characteristics, using equipment of the Shared Research Center of the Federal Scientific Research Centre "Crystallography and Photonics" of the Russian Academy of Sciences.

## REFERENCES

1. A. D. Kirhenbaum and J. A. Cahill, J. Inorg. Nucl. Chem. **14** (1–2), 148 (1960).
2. N. I. Sorokin, M. V. Fominykh, E. A. Krivandina, et al., Crystallogr. Rep. **41** (2), 292 (1996).

3. N. I. Sorokin and B. P. Sobolev, Elektrokhimiya **43** (4), 420 (2007).
4. N. I. Sorokin and B. P. Sobolev, Kristallografiya **39** (5), 889 (1994).
5. B. P. Sobolev and N. I. Sorokin, Crystallogr. Rep. **59** (6), 807 (2014).
6. B. P. Sobolev, N. I. Sorokin, and N. B. Bolotina, *Photonic and Electronic Properties of Fluoride Materials,* Ed. by A. Tressaud and K. Poeppelmeier (Elsevier, Amsterdam, 2016), p. 465.
7. O. Greis and M. S. R. Cader, Thermochim. Acta **87**, 145 (1985).
8. K. Rotereau, Ph. Daniely, A. Desert, and J. Y. Gesland, J. Phys. Cond. Matter **10** (6), 1431 (1998).
9. B. P. Sobolev, *The Rare Earth Trifluorides. The High Temperature Chemistry of Rare Earth Trifluorides* (Institut d'Estudis Catalans, Barcelona, 2000).
10. A. A. Potanin, Zh. Ross. Khim. O-va im. D. I. Mendeleeva **XLV** (5–6), 58 (2001).
11. M. Anji Reddy and M. Fichtner, J. Mater. Chem. **21**, 17059 (2011).
12. C. Rongeat, M. Anji Reddy, R. Witter, and M. Fichtner, J. Phys. Chem. **117**, 4943 (2013).
13. F. Gschwind, G. Rodriguez-Garsia, D. J. S. Sandbeck, et al., J. Fluor. Chem. **182**, 76 (2016).
14. B. Dieudonne, J. Chable, F. Mauvy, et al., J. Phys. Chem. C **119**, 25170 (2015).
15. B. P. Sobolev and K. B. Seiranian, J. Solid State Chem. **39** (3), 337 (1981).
16. B. P. Sobolev, D. N. Karimov, D. N. Sul'yanov, et al., Crystallogr. Rep. **54** (1), 122 (2009).
17. N. I. Sorokin, D. N. Karimov, E. A. Sul'yanova, et al., Crystallogr. Rep. **55** (4), 662 (2010).
18. A. Roos, A. F. Aalders, J. Schoonman, et al., Solid State Ionics **9–10**, 571 (1983).
19. N. I. Sorokin and B. P. Sobolev, Elektrokhimiya **43** (4), 420 (2007).
20. A. K. Ivanov-Shits, N. I. Sorokin, P. P. Fedorov, and B. P. Sobolev, Fiz. Tverd. Tela **25** (6), 1748 (1983).
21. B. P. Sobolev, V. B. Aleksandrov, P. P. Fedorov, et al., Kristallografiya **21** (1), 95 (1976).
22. N. B. Bolotina, T. S. Chernaya, A. I. Kalyukanov, et al., Crystallogr. Rep. **60** (3), 346 (2015).
23. O. N. Khrykina, N. I. Sorokin, I. A. Verin, et al., Crystallogr. Rep. **62** (4), 545 (2017).
24. L. R. Batsanova, Usp. Khim. **40** (6), 945 (1971).
25. G. V. Anan'eva, E. N. Baranova, M. N. Zarzhitskaya, et al., Izv. Akad. Nauk SSSR, Neorg. Mater. **16** (1), 68 (1980).
26. E. Staritzky and L. B. Asprey, Anal. Chem. **29** (5), 855 (1957).
27. E. A. Radzhabov and V. A. Kozlovskii, Bull. Russ. Acad. Sci.: Phys. **79** (2), 251 (2015).
28. I. V. Murin, O. V. Glumov, I. G. Podkolzina, et al., Zh. Prikl. Khim. **55** (2), 300 (1982).
29. A. I. Livshits, V. M. Buznik, P. P. Fedorov, and B. P. Sobolev, Neorg. Mater. **18** (1), 135 (1982).
30. A. F. Aalders, A. Polman, A. F. M. Arts, and H. W. de Wijn, Solid State Ionics **9–10**, 539 (1983).
31. M. A. Denecke, W. Gunser, A. V. Privalov, and I. V. Murin, Solid State Ionics **52**, 327 (1992).
32. T. Takahashi, H. Iwahara, and T. Ishikawa, J. Electrochem. Soc. **124** (2), 280 (1977).
33. I. V. Murin, O. V. Glumov, and Yu. V. Amelin, Zh. Prikl. Khim. **53** (7), 1474 (1980).
34. A. Roos, F. C. M. van de Pol, R. Keim, and J. Schoonman, Solid State Ionics **13**, 191 (1984).

*Translated by Yu. Sin'kov*